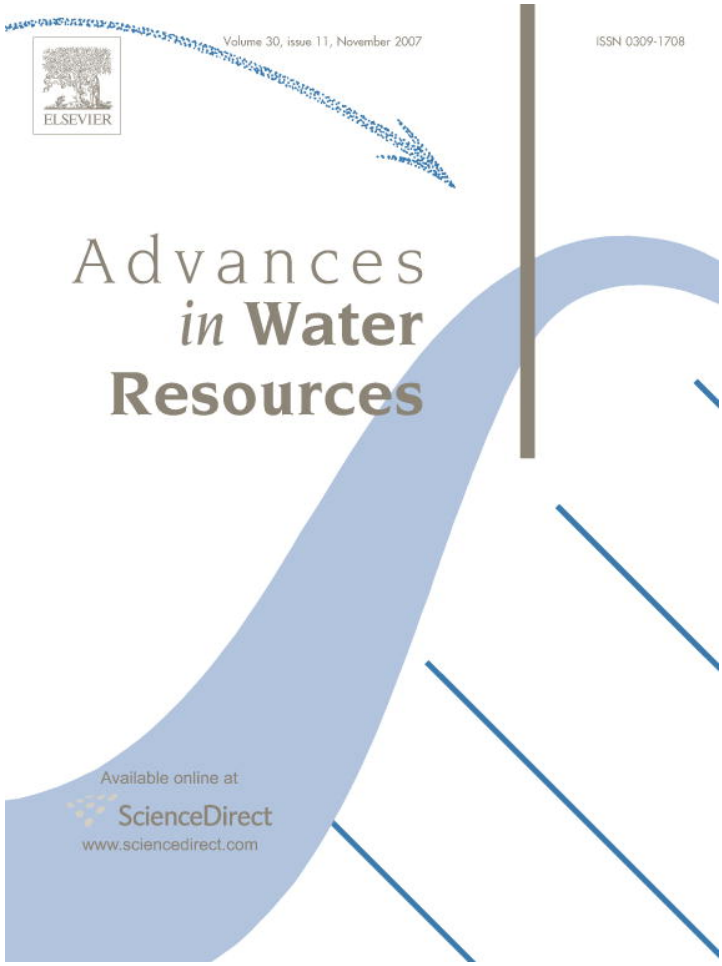

Available online at www.sciencedirect.com
ScienceDirect
Advances in Water Resources 30 (2007) 2387–2399
Advances in Water Resources
www.elsevier.com/locate/advwatres

Diagnosing peak-discharge power laws observed in rainfall–runoff events in Goodwin Creek experimental watershed

Peter R. Furey [a,*], Vijay K. Gupta [b]

[a] NorthWest Research Associates/CORA, 3380 Mitchell Lane, Boulder, CO 80301, United States
[b] Department of Civil and Environmental Engineering, Cooperative Institute for Research in Environmental Sciences, University of Colorado, Boulder, United States

Received 1 September 2006; received in revised form 25 May 2007; accepted 28 May 2007
Available online 10 June 2007

Abstract

Observations from the Goodwin Creek experimental watershed (GCEW), Mississippi show that peak-discharge $Q(A)$ and drainage area A are related, on average, by a power law or scaling relationship, $Q(A) = \alpha A^{\theta}$, during single rainfall–runoff events. Observations also show that α and θ change between events, and, based on a recent analysis of 148 events, observations indicate that α and θ change because of corresponding changes in the depth, duration, and spatial variability of excess-rainfall. To improve our physical understanding of these observations, a 5-step framework for diagnosing observed power laws, or other space-time patterns in a basin, is articulated and applied to GCEW using a combination of analysis and numerical simulations. Diagnostic results indicate how the power laws are connected to physical conditions and processes. Derived expressions for α and θ show that if excess-rainfall depth is fixed then there is a decreasing concave relationship between α and excess-rainfall duration, and an increasing and slightly convex relationship between θ and excess rainfall duration. These trends are consistent with observations only when hillslope velocity v_h is given a physically realistic value near 0.1 m/s. If $v_h \gg 0.1$ m/s, then the predicted trends deviate from observed trends. Results also suggest that trends in α and θ can be impacted by the dependence of v_h and link velocity v_l on excess-rainfall rate.

Keywords: Peak-discharge; Floods; Power laws; Scaling; Excess rainfall

1. Introduction

Ogden and Dawdy [20] observed that peak stream discharge $Q(A)$ and drainage area A for individual rainfall–runoff events in the 21 km^2 Goodwin Creek experimental watershed (GCEW) in Mississippi are related, on average, by a power law $Q(A) = \alpha A^{\theta}$. They also observed that α and θ change among events. This surprising discovery showed for the first time that spatial power laws in peak-discharge are present in a real basin on an event-by-event basis. Power laws arise in scale-invariant systems, and therefore represent a robust signature in data [9]. Until the Ogden and Dawdy paper was published, peak streamflow power laws for events had been shown to hold only for idealized mean self-similar basins under idealized physical conditions [8,16]. These studies did not report on event-to-event variability in scaling parameters as Ogden and Dawdy found in data.

Furey and Gupta [5] analyzed 148 events in GCEW to understand the physical origins of the temporal variability in α and θ that Ogden and Dawdy [20] observed. For each event, they evaluated the depth and duration of estimated excess rainfall, denoted by $\hat{r}_d$ and $\hat{\sigma} = \hat{r}_d/\hat{r}_p$ where $\hat{r}_p$ is the peak of estimated excess-rainfall. They observed the following trends among the events:

1. For events with the same duration $\hat{\sigma}$, α increased and θ remained constant as depth $\hat{r}_d$ increased. The relationship between α and $\hat{r}_d$ was linear.
2. For events with the same depth $\hat{r}_d$, α decreased and θ increased as duration $\hat{\sigma}$ increased. These relationships were nonlinear.

* Corresponding author.
E-mail address: furey@cora.nwra.com (P.R. Furey).

0309-1708/$ - see front matter © 2007 Elsevier Ltd. All rights reserved.
doi:10.1016/j.advwatres.2007.05.014

In trend 2, the relationship between α and $\hat{\sigma}$ was based on data points having considerable variability and was more speculative than definitive. The relationship between θ and $\hat{\sigma}$ has been predicted theoretically under idealized conditions.

The objective of this paper is to extend our physical understanding of the observed power laws in GCEW. Following Klemes [11] and Gupta et al. [9], we pursue this objective using a diagnostic framework. Klemes [11] has illustrated the conceptual difference between a diagnostic framework for improving a physical model and a model that is fitted to data by calibration. Gupta et al. [9] give an overview of progress that has been made in the last 20 years in understanding the physical origins of spatial power laws that are observed, on average, in floods. The time scales represented by these power laws range from hours and days for individual flood events to years for annual flood frequencies. The article argues that a diagnostic framework is necessary to understand how power laws in floods arise from physical processes and to develop reliable models for flood prediction in ungauged basins.

The diagnostic framework that guides our objective is not specific to GCEW and can be applied to understanding space-time patterns in any basin. It consists of five steps:

1. Identify and quantify a recurring space-time pattern in data.
2. Use datasets that complement the data in step 1 to show, qualitatively, how certain conditions and processes influence the pattern.
3. Develop theoretical expressions and/or run simulations to describe how the pattern depends on the conditions and physical processes examined in step 2.
4. Test the results of step 3 against those in step 2.
5. Assess the test results from step 4 and repeat, if necessary, steps 2–5.

A model requiring calibration should not be used to pursue step 3. Therefore, the word 'simulations' is used in explaining this step. Step 5 is an assessment of how well the physical origin of the recurring pattern has been explained and provides a basis for introducing more complexity, if necessary, into steps 2 and 3.

Ogden and Dawdy [20] took step 1 in their investigation of peak stream discharge in GCEW. The recurring space-time pattern they identified is a power law in peak-discharge that is present from event-to-event in GCEW. They used a least-squares linear regression to quantify the power law parameters α and θ.

Furey and Gupta [5] took step 2. Guided by past research results and using a combination of streamflow and rainfall data, they showed, qualitatively, how the depth and duration of estimated excess rainfall influences peak-discharge power laws in GCEW. Their findings are summarized above.

In this paper, we take steps 3–5 in our diagnostic framework. For step 3, we develop a simple space-time expression for the peak of mean discharge as a function of drainage area, excess-rainfall depth, and excess-rainfall duration. This expression provides a basis for understanding the observations presented in [5,20]. Our expression is derived from a convolution equation for mean discharge that is a spatial generalization of the geomorphologic instantaneous unit hydrograph (GIUH). We use a GIUH representation of streamflow because rainfall over GCEW tends to be spatially uniform [20]. In our convolution equation, mean discharge is conditioned on the duration of excess-rainfall and the duration of hydrological response for an instantaneous input of excess rainfall over a basin. The hydrological response depends on drainage area. The input function represents the conditional mean shape of the excess-rainfall time series during a rainfall–runoff event in GCEW. The response function represents the conditional mean shape of the hydrological response time series formed by an instantaneous input of excess-rainfall. A combination of data and simulation results are used to define the input and response functions. For example, the duration of hydrological response is parameterized in terms of drainage area using numerical simulations. The convolution equation describes the mean hydrograph at any location in GCEW, not just the outlet, for a rainfall–runoff event. To pursue steps 4 and 5, we tested our expression for the peak of mean discharge against the power law trends reported in [5] and listed above.

This paper is organized as follows. In Section 2, research results are discussed which indicate that peak streamflows are scale invariant in space during single rainfall–runoff events. In Section 3, certain basic features of estimated mean excess-rainfall time series and mean simulated basin-response functions in GCEW are evaluated. Then, based on these features, an equation for mean discharge is developed in Section 4 that is a spatial and statistical generalization of GIUH. A peak-discharge equation is obtained by taking the maximum of the mean discharge equation. In Section 5, predictions made by the peak-discharge equation are compared with observational results of peak flows in GCEW that are presented in Furey and Gupta [5]. The observational results show how the mean of peak streamflow relates to spatial scale. By contrast, our theory describes how the maximum of mean streamflow relates to spatial scale. Consequently, our theory only provides a qualitative physical understanding of the observational results because mean of the maximum is not the same as maximum of the mean. A summary of findings are given in Section 6. Appendix A lists the definitions of the mathematical symbols used in Sections 3–5.

2. Background

A scaling theory of floods has been developing since Gupta et al. [7] published a first paper on it. The goal of the theory is first to understand how spatial peak-discharge power laws are connected to physical processes during rainfall–runoff events, and then to extend this understanding to

longer time scales. Results in [7] have been generalized in many directions for idealized mean self-similar channel networks [8,16,17,19,29,30]. However, there is a pressing need to generalize the scaling theory to real channel networks and test it against event-based rainfall–runoff data [9]. For this purpose, basins with a large number of rainfall and streamflow gauges that operate concurrently are required for testing the predictions of the theory against observations. Unfortunately, there are only a few gauged basins in the world that can be used for this purpose. These issues make the problem of extending the theory from idealized to real networks a major scientific challenge that requires new advances both on observational and theoretical fronts.

2.1. Goodwin Creek experimental watershed (GCEW)

GCEW is one of only a few basins in the world that consists of a dense network of rainfall gauges that are sampled simultaneously with streamflow gauges [1]. It has a drainage area of 21.2 km^2 and is located near Batesville, MS. Streamflows are measured in flumes located at 14 nested subbasins [2]. Rainfall is measured at 31 locations in or near the basin using standard tipping-bucket and weighing rain gauges [27]. Rainfall and streamflow measurements have been recorded since the end of 1981. All streamflow and rainfall gauges are operated by the US Department of Agriculture, Agricultural Research Service (ARS), National Sedimentation Laboratory [2]. Drainage areas of the stream gauges range from 0.172 km^2 for gauge 9 to 21.2 km^2 for gauge 1 at the basin outlet. Perennial streamflow occurs in the lower reaches of GCEW, but most streamflow is ephemeral in the basin. Streamflow quickly exits the basin during a rainstorm with prestorm streamflow levels returning within one to three days [2]. The dominant runoff process in GCEW is Hortonian overland flow. Groundwater levels taken beside the main channel of the basin show that the water table is several meters deep while channels throughout the basin are incised 2–3 m on average. Base flow at the outlet tends to be less than 0.05 m^3/s [20]. In summary, GCEW is an ideal basin for studying how streamflows change in space because it has an extensive spatial network of rainfall and streamflow gauges, and runoff generation in the basin is largely controlled by relatively simple hydrological conditions.

2.2. Spatial scale-invariance in peak streamflows in terms of conditional mean response formulations

Real channel networks exhibit spatial statistical variability, and rainfall time series exhibit temporal statistical variability during rainfall–runoff events. These two features require that even the simplest convolution-type representation of streamflow be treated as a stochastic integral. The first steps to make progress on this complex problem considered mean streamflow expressions conditioned on drainage magnitude. For example, Troutman and Karlinger [28] derived an asymptotic expression for the mean width function conditioned on network magnitude using Shreve's [24] random network model. Gupta and Waymire [8] used this expression in a convolution to compute the scaling exponents for floods. They assumed that the mean input function represents a spatially uniform and temporally constant rainfall intensity with a finite duration.

Results in [8] show three prominent features in peak flow scaling for an event in a large "parent" basin: (1) for small subbasins (below a certain magnitude threshold), there is a power law relationship between peak flows and basin magnitude with an exponent near 1; (2) for large subbasins (above a certain magnitude threshold) there is a second power law with an exponent of 0.5; (3) for intermediate size basins (between the small and large subbasin thresholds) the relationship between peak flows and basin magnitude is in transition between the power laws described by (1) and (2). These three features carry over to peak flows and drainage area assuming that area is proportional to magnitude. They are presented in this context by Sivapalan et al. [25] using a simple model of basin response. These scaling features have been observed in a few rainfall–runoff events in the Walnut Gulch basin, AZ [9]. While they are for single rainfall–runoff events, these features have also been observed in annual flood frequencies in the Walnut Gulch basin [6]. The observed power laws for GCEW probably represent features (1) and (3), but not (2) because the basin is relatively small.

To take step 3 in our diagnostic framework, a description of the mean GIUH conditioned on drainage area is needed for GCEW. However, there are currently no analytical results that can describe either the width function or the mean GIUH conditioned on drainage area for real river networks. Therefore, as explained below, certain basic features of estimated mean excess-rainfall time series and mean simulated basin-response functions in GCEW are evaluated. Based on these features, a conditional equation for expected stream discharge and a conditional equation for the peak of expected discharge are developed for GCEW.

3. Characteristics of mean excess-rainfall time series and mean basin-response functions in GCEW

To develop a general expression for stream discharge in GCEW, we first evaluated three characteristics of the basin: (1) the general shape of the mean excess-rainfall time series in the basin during a rainfall–runoff event, (2) the general shape of the basin's mean response function, and (3) the way that the response function is parameterized with respect to drainage area. As explained below, these three characteristics were evaluated from conditional mean time series of estimated excess-rainfall and conditional mean functions for simulated basin-response.

3.1. Using data to assess the mean shape of excess-rainfall time series

The mean shape of excess-rainfall time series in GCEW was assessed using estimated time series for each of 148

rainfall–runoff events in the basin [5]. A time series was estimated for an event by applying the Phi-Index Method to spatially-averaged rainfall and streamflow data from the outlet of the basin [14]. The approach and results of this estimation are discussed in Furey and Gupta [5]. Following [5], we evaluated the excess-rainfall duration for each time series using a surrogate measure defined as $\hat{\sigma} = \hat{r}_d/\hat{r}_p$ where $\hat{r}_d$ is the depth of estimated excess-rainfall (mm) and $\hat{r}_p$ is the peak of estimated excess-rainfall (mm/h).

A mean excess-rainfall time series was evaluated by conditioning the events on a narrow range of $\hat{\sigma}$ values. Fig. 1 illustrates the problem that arises when evaluating a mean time series without conditioning; it also arises when evaluating a mean function for basin-response. Note that Eagleson [4] conditioned on storm duration to develop expressions for the probability density of mean storm intensity and total storm depth. However, unlike [4], our goal is to evaluate the properties of mean excess-rainfall time series and mean-response functions for single events.

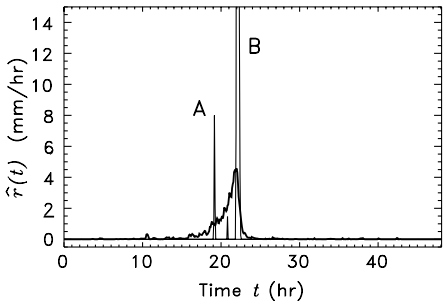

Fig. 1. The mean time series of estimated excess-rainfall for the 148 events in GCEW (dark curve) and time series from two events in the group denoted A and B. The mean time series poorly represents both the duration and peak of the time series for the two events shown.

Excess-rainfall time series, conditioned on a range of $\hat{\sigma}$ values, must be centered on a common feature to produce a mean time series from them. One approach is to center the time series on their peaks, so that each excess-rainfall peak occurs at the same moment in time. A second approach is to center the excess-rainfall time series on the streamflow peaks, recorded at the outlet of GCEW, to which they correspond. Regardless of which centering approach is used to evaluate a mean excess-rainfall time series, we found that a Gaussian function is a reasonable first-order approximation for the general shape of the mean time series of excess-rainfall in GCEW conditioned on duration.

Fig. 2 shows the results of our conditional analysis for the second centering approach discussed above. Plots at the top of the figure show the estimated excess-rainfall rate $\hat{r}(t)$ versus time t conditioned on a narrow range of $\hat{\sigma}$ values. In each plot, there are n time series of $\hat{r}(t)$. For each time series, the corresponding peak streamflow at the outlet of GCEW occurs at $t = 24$; thus, time is centered on ± 24 h from the time of peak streamflow at the outlet of GCEW. Plots at the bottom show the mean time series of $\hat{r}(t)$, calculated from each plot at the top, and a corresponding fitted Gaussian density function. Qualitatively, a Gaussian density captures the overall time series pattern for each group. This result is also found for other groups of $\hat{\sigma}$. Note that the value of r_d/r_p for the Gaussian function is larger than the value of $\hat{\sigma} = \hat{r}_d/\hat{r}_p$ on which events have been con-

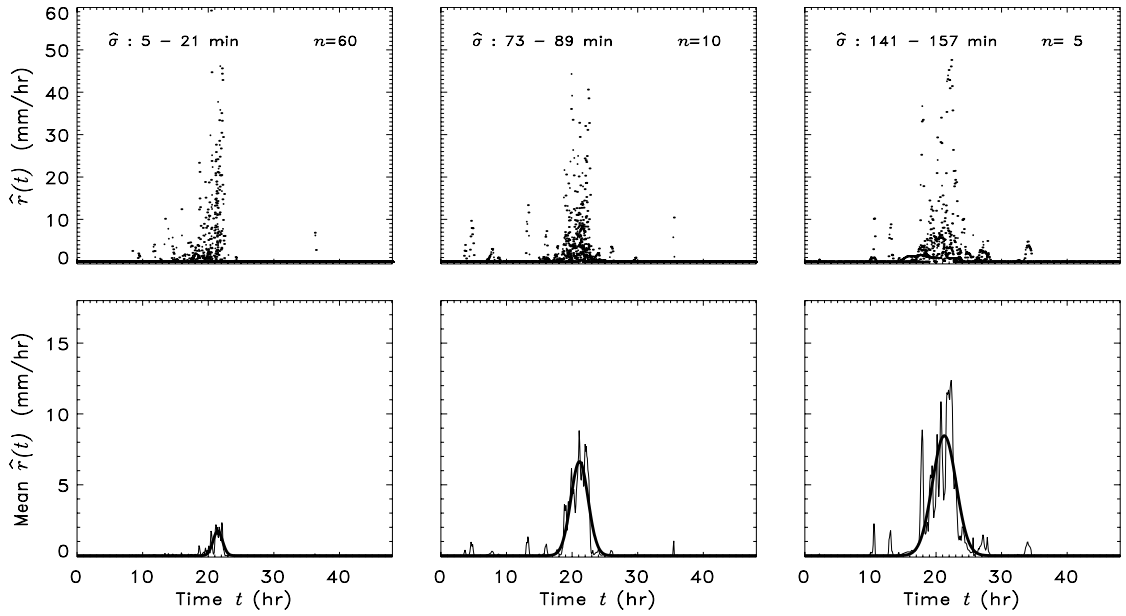

Fig. 2. Top plots show values of $\hat{r}(t)$ versus t conditioned on a narrow range of values for the estimated duration of excess-rainfall, $\hat{\sigma}$. In each plot, there are n time series of $\hat{r}(t)$. For each time series, the corresponding peak streamflow at the outlet of GCEW occurs at $t = 24$; thus, time is centered on ± 24 h from the time of peak streamflow at the outlet. Points for each time series are unconnected to preserve graphical clarity. Bottom plots show corresponding mean values of $\hat{r}(t)$ versus t (thin line) and a fitted Gaussian density function (thick line).

ditioned. A possible cause for this discrepancy is that the velocity of surface runoff changes between events.

3.2. Using a GIS-based simulation to assess the mean shape of basin-response functions

A GIS-based numerical simulation software called CUENCAS was used to simulate streamflow $q(t, A)$ throughout GCEW to determine the mean shape of the basin's response functions. Simulations were limited to a few basic physical processes and conditions in order to gain an understanding of their interaction and influence. The topography of GCEW was represented by a DEM of 30 m resolution, which Mantilla and Gupta [15] found to be the lowest resolution that can accurately characterize the network structure of a basin. The river network was extracted from the DEM using CUENCAS and compared well with Blue Line maps of the basin. An 'instantaneous' pulse of excess rainfall with a depth of 0.001 m (1 mm) was used to force a simulation. To represent this pulse, each hillslope in GCEW was covered uniformly with water having a depth of 0.001 m and then the basin was allowed to drain. A linear storage–discharge relationship with flow velocity v_h was used to characterize runoff from a hillslope. Likewise, a linear storage–discharge relationship with flow velocity v_l was used to characterize runoff from a link. Hillslope and link dynamics included storage attenuation, and simulated streamflow $q(t, A)$ was sampled at each outlet of the 552 links that comprise the DEM-extracted river network.

Under the conditions described above, a simulated hydrograph for a given subbasin in GCEW is a GIUH. Therefore, a simulation produced a family of 552 GIUH's characterizing the sampled subbasins and outlet of GCEW. This family of GIUH's was viewed as a family of response functions, with each response function determined by flow dynamics and network structure.

Fig. 3 shows the results of our conditional analysis on simulations where $v_h = 0.1$ m/s and $v_l = 1$ m/s. To make this Figure, we first defined a range of areas A and then a range of basin-response durations on which to condition our analysis. We evaluated the duration for each subbasin using a surrogate measure defined as $\tau = q_T(A)/Q(A)$ where $q_T(A) = 0.001A$ is the total discharge volume (m^3) and $Q(A)$ is the simulated discharge peak (m^3/s). Notice that τ is comparable to $\hat{\sigma}$ discussed in Section 3.1. The three plots at the top of Fig. 3 show $q(t, A)$ versus t conditioned on a range of A and τ values. The third plot includes the response function for the outlet of GCEW. Plots at the bottom show the mean time series of $q(t, A)$, calculated from each plot at the top, and a corresponding fitted Gaussian density function. Qualitatively, a Gaussian density captures the mean time series pattern for each group. This result is also found for other groups of A and τ. This exercise illustrates that a Gaussian density function is a reasonable first-order approximation for the shape of the conditional mean basin-response function when $v_h = 0.1$ m/s and $v_l = 1$ m/s. Simulations using other values for v_h and v_l lead to the same conclusion.

3.3. Parameterizing the relationship between the duration of the mean basin-response function and drainage area

To examine how the response function in GCEW changes with respect to drainage area, each value of τ obtained from a simulation was plotted against A in log–log space. Three simulations were run where $v_h = 0.1$, 1.0, and ∞ m/s and

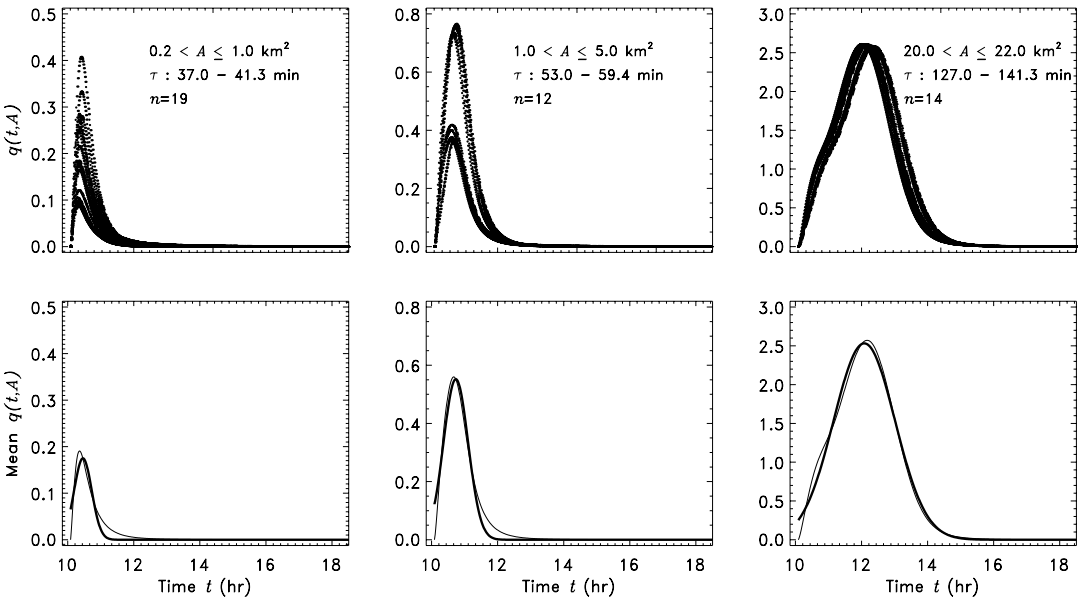

Fig. 3. Simulation results where $v_h = 0.1$ and $v_l = 1.0$ m/s. The first three plots (top) show values of simulated discharge $q(t, A)$ versus t conditioned on a narrow range of values for both A and the estimated duration of the simulated streamflow response, τ. In log space, the size of the range for A is the same for the first two plots. The third plot (top) includes $q(t, A)$ versus t at the outlet of GCEW. The number of hydrographs per plot is indicated by n. Bottom plots show corresponding mean values of $q(t, A)$ versus t (thin line) and a fitted Gaussian density function (thick line).

$v_l = 1$ m/s. The condition where $v_h = \infty$ means that all of the water on each hillslope flows instantaneously to its adjoining link; thus, hillslopes do not affect basin response. Fig. 4 shows how τ and A are related for each simulation scenario and that the relationship appears to become log–log linear as A increases. For basins of order $\omega \geqslant 2$, the relationship between τ and A is captured, on average, by a power law $\tau = cA^{\lambda}$. This relationship holds for other values of v_l and is used to develop a generalized GIUH in Section 4. Sivapalan et al. [25] and Sólyom and Tucker [26] have developed peak flow equations using a similar relationship.

Power law parameters in the relationship $\tau = cA^{\lambda}$ are sensitive to surface routing conditions. As shown in Fig. 4, c decreases and λ increases as hillslope velocity v_h increases. On the otherhand, c and λ remain the same if, for example, the initial excess-rainfall depth is changed from 1 to 5 mm.

The relationship $\tau = cA^{\lambda}$ is closely related to the shape and scale of width functions in GCEW. First, a similar relationship between τ and A for basins of order $\omega \geqslant 2$ is

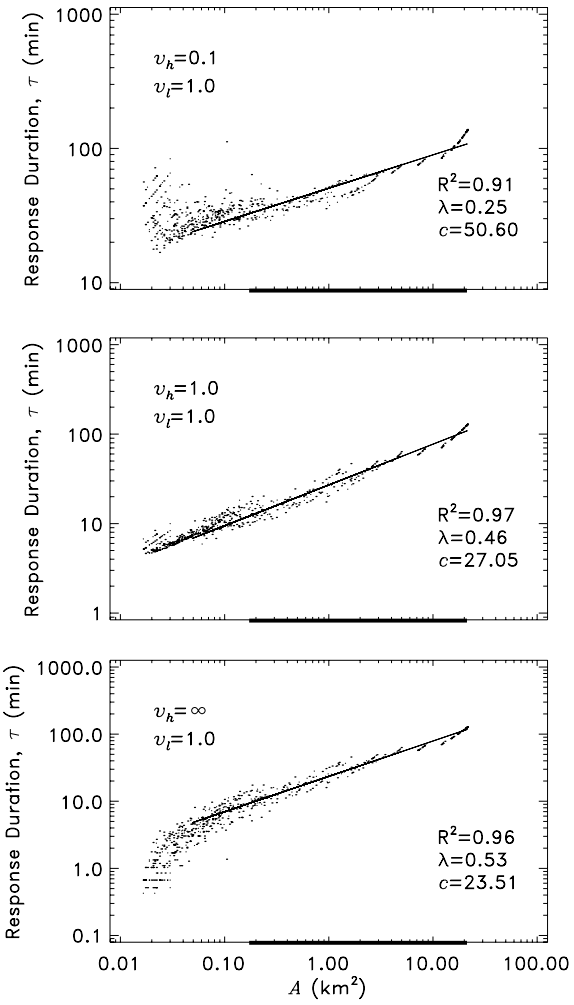

Fig. 4. Duration of simulated basin-response τ versus A in log–log space for $v_h = 0.1$, 1.0, and ∞ m/s (top to bottom) and $v_l = 1.0$ m/s. The line is fitted to points from basins of order $\omega \geqslant 2$ and indicates that, to a first-order, $\tau = cA^{\lambda}$. The thick line on the x-axis depicts the range of spatial scales represented by stream gauges in GCEW.

obtained for a simulation where $v_h = \infty$ and channeled water in GCEW is routed translationally with constant velocity and no storage attenuation. In this situation, the hydrograph for a subbasin in GCEW is equivalent to the width function for that subbasin, and, by extension, the relationship between τ and A can be obtained directly from width functions. Second, multiplying $\tau = cA^{\lambda}$ by a constant velocity v gives a relationship between distance $v\tau$ and A that is comparable to Hack's Law [9,10,18,22,23]. Hack's Law for GCEW using basins of order $\omega \geqslant 2$ gives $L \propto A^{0.63}$ where L is defined as the longest channel length in a basin and equals the basal length of its width function.

4. A space-time representation of mean streamflow

We use the observations presented in Sections 3.1, 3.2 and 3.3 to develop a spatial-mean GIUH. To summarize, these observations show that: (1) the mean time series of excess-rainfall when conditioned on duration can be approximated by a Gaussian density function; (2) the mean basin-response function when conditioned on duration can be approximated by a Gaussian density function; and (3) a power law connects the mean duration of basin-response to drainage area.

We also assume that excess-rainfall in GCEW is uniform in space but variable in time during rainfall–runoff events. The basis for this assumption is that the correlation length scale of spatial rainfall in and around GCEW is observed to be ~40 km while the greatest distance across the basin is ~8 km [20]. This assumption is not expected to be valid for events where the spatial variability in soil-moisture is large because this condition can produce a large spatial variability in excess-rainfall.

4.1. Expected discharge from a basin

Discharge from a basin of drainage area A can be expressed as

$$Q_A(t) = \frac{v}{l}\int_0^T R(s)W_A(v(t-s)/l)\,\mathrm{d}s; \quad 0 < T < t, \tag{1}$$

where the integral is a convolution in time t and represents storage in the outlet link of the basin. Here, $R(s)$ is a stochastic process that represents the excess-rainfall that enters a channel from a hillslope during a single rainfall–runoff event in the basin; $W_A(v(t-s)/l)$ is a stochastic process representing the basin's response during an event; v represents an effective runoff velocity for the basin; l is the mean distance that water travels through a network link; and T is the duration of a rainfall–runoff event. An event starts when excess-rainfall generation begins and ends when streamflow response finishes. Runoff velocity v is assumed to be constant in time during a single rainfall–runoff event. This assumption is made to simplify mathematics and means that a change in discharge at the outlet of a basin with drainage area A will correspond to a change in streamflow depth and/or width at the outlet. This is not an unreasonable simplification be-

cause the product of depth and width changes more than velocity as discharge increases at a station [13].

To develop a space-time formulation of discharge, take the conditional expectation of Eq. (1) to get

$$E[Q_A(t)|D_1, D_{2,A}] = \frac{v}{l}\int_0^T E[R(s)|D_1]E[W_A(v(t-s)/l)|D_{2,A}]\,\mathrm{d}s, \tag{2}$$

where $E[Q_A(t)|D_1, D_{2,A}]$ is the expected discharge for a basin of drainage area A conditioned on the duration of excess-rainfall D_1 and the duration of the basin-response function $D_{2,A}$. Subscripts 1 and 2 are used to distinguish between the two types of durations. Subscript A shows that the duration of the basin-response function depends on spatial scale. Using duration as the conditional parameter is based on the observations presented in Section 3. Eq. (2) assumes that time series of excess-rainfall are statistically independent of the response functions in a basin.

4.2. Explicit representations of mean excess-rainfall and mean basin-response

Explicit representations of $E[R(s)|D_1]$ and $E[W_A(v(t-s)/l)|D_{2,A}]$ are needed to solve Eq. (2). Based on the observations presented in Sections 3.1 and 3.2, we relate these terms to Gaussian density functions. First, assume that

$$E[R(s)|D_1] = E[Z|D_1]af_1(s), \tag{3}$$

where $E[Z|D_1]$ is the expected total depth of excess-rainfall given D_1, a is the mean area of all hillslopes that drain into the links in a basin, s is time since the beginning of the event, and $f_1(s)$ is a normal density function with parameters μ_1 and σ_1. The parameter σ_1 is a measure for the duration of the expected time series of excess-rainfall. If the value of D_1 is fixed, then theoretically the value of σ_1 is fixed as well. The parameters μ_1 and σ_1 have units of time giving $E[R(s)|D_1]$ the unit volume per time. Integrating (3) over t gives the expected volume of rainfall over the mean hill area, $E[Z|D_1]a$.

Second, assume that

$$\begin{aligned} E[W_A(v(t-s)/l)|D_{2,A}] &= (ln/v)f_{2,A}(t-s) \\ &= (lA/va)f_{2,A}(t-s), \end{aligned} \tag{4}$$

where n is the total number of links in a basin of area A, $f_{2,A}(t-s)$ is a normal density function with mean $\mu_{2,A}$ and standard deviation $\sigma_{2,A}$. The parameter $\sigma_{2,A}$ is a measure for the duration of the expected response function. If the value of $D_{2,A}$ is fixed, then theoretically the value of $\sigma_{2,A}$ is fixed as well. Here, $E[W_A(v(t-s)/l)|\ D_{2,A}]$ is dimensionless and the second equality follows by assuming that drainage density is the constant l/a.

Simulated response functions for GCEW change in shape with an increase in spatial scale. This change in shape is expressed, on average, by a power law as $\tau = cA^{\lambda}$; see Section 3.3. Although Eq. (4) shows that the expected response function changes with A, it does not explicitly capture this change-in-shape feature. Therefore, to include this feature, first define $\overline{D}_{2,A} = E[D_{2,A}]$ and define $\bar{f}_{2,A}$ as the normal density function with mean $\bar{\mu}_{2,A}$ and standard deviation $\bar{\sigma}_{2,A}$ that corresponds to $\overline{D}_{2,A}$. Then, equating τ from our simulations with $\bar{\sigma}_{2,A}$, assume that $\bar{\sigma}_{2,A} = cA^{\lambda}$ where c and $0 \leqslant \lambda < 1$ are constants and are independent of A. Accordingly, the expectation of the response function conditioned on $\overline{D}_{2,A}$ is

$$E[W_A(v(t-s)/l)|\overline{D}_{2,A}] = (lA/va)\bar{f}_{2,A}(t-s), \tag{5}$$

where $\bar{\sigma}_{2,A} = cA^{\lambda}$ in $\bar{f}_{2,A}(t-s)$. As mentioned in Section 3.3, Sivapalan et al. [25] and Sólyom and Tucker [26] developed peak flow equations using travel-time relationships that are comparable to $\bar{\sigma}_{2,A} = cA^{\lambda}$.

Eq. (5) indicates that the basin-response function changes non-linearly with spatial scale among nested basins. This result can be seen by writing out (5) and evaluating its maximum to get

$$\max_t E[W_A(vt/l)|\overline{D}_{2,A}] = \frac{lA}{\sqrt{2\pi}va\bar{\sigma}_{2,A}} = \frac{lA^{1-\lambda}}{\sqrt{2\pi}vac}. \tag{6}$$

This expression shows that the peak of the expected basin-response function changes with area as $A^{1-\lambda}$. Veitzer and Gupta [30] reported a similar empirical relationship between the expected value of the width function peaks and A.

4.3. Expression for mean space-time discharge

Substituting (3) and (5) into (2) gives

$$E[Q_A(t)|D_1, \overline{D}_{2,A}] = E[Z|D_1]A\int_0^T f_1(s)\bar{f}_{2,A}(t-s)\,\mathrm{d}s. \tag{7}$$

The integral in (7) can be expressed as

$$\begin{aligned} \int_0^T f_1(s)\bar{f}_{2,A}(t-s)\,\mathrm{d}s &= \frac{1}{2\pi\sigma_1\bar{\sigma}_{2,A}}\int_0^T \exp\left(\frac{-(s-\mu_1)^2}{2\sigma_1^2}\right)\exp\left(\frac{-(t-s-\bar{\mu}_{2,A})^2}{2\bar{\sigma}_{2,A}^2}\right)\mathrm{d}s \\ &= \frac{1}{\sqrt{2\pi\left(\sigma_1^2+\bar{\sigma}_{2,A}^2\right)}}\exp\left(\frac{-(\mu_1-\beta)^2}{2(\sigma_1^2+\bar{\sigma}_{2,A}^2)}\right)\int_0^T \frac{1}{\sqrt{2\pi}\delta}\exp\left(\frac{-(s-\gamma)^2}{2\delta^2}\right)\mathrm{d}s, \end{aligned} \tag{8}$$

where $\beta = t - \bar{\mu}_{2,A}$, $\gamma = (\mu_1\bar{\sigma}^2_{2,A} + \bar{\mu}_{2,A}\sigma^2_1)/(\sigma^2_1 + \bar{\sigma}^2_{2,A})$, and $\delta = \sigma_1\bar{\sigma}_{2,A}/(\sigma^2_1 + \bar{\sigma}^2_{2,A})$. In the first equality, the numerator of the second exponential term is $-(t-s-\bar{\mu}_{2,A})^2 = -((-1)(s-t+\bar{\mu}_{2,A}))^2 = -(s-t+\bar{\mu}_{2,A})^2$. By substituting in this relationship, the second equality in (8) can be derived using an expression for the product of two exponential functions that is found in Parzen (pg. 191) [21].

To develop our final expression for $E[Q_A(t)|D_1, \overline{D}_{2,A}]$, we let the duration of a rainfall–runoff event $T = 2\gamma$ where $\gamma > 2\delta$. Under this condition, the integral in the second equality in (8) is approximately one because the integrand is a normal density function. Therefore, combining Eqs. (7) and (8) gives

$$E[Q_A(t)|D_1, \overline{D}_{2,A}] = \frac{E[Z|D_1]A}{\sqrt{2\pi\left(\sigma^2_1 + \bar{\sigma}^2_{2,A}\right)}} \exp\left(\frac{-(t-\mu_1-\bar{\mu}_{2,A})^2}{2(\sigma^2_1+\bar{\sigma}^2_{2,A})}\right). \tag{9}$$

This equation explicitly shows that the response function of a basin changes in shape with spatial scale because $\bar{\sigma}_{2,A} = cA^{\lambda}$. It can be viewed as a lumped hydrological model because model parameters are spatial-mean values. More complicated models have been formulated that include, for example, a temporally-variable source area for excess-rainfall generation and a spatially variable channel-roughness coefficient; e.g. [12]. However, such models have many parameters and rely on statistical multiple-regression relationships instead of physically-based relationships. We have purposefully developed Eq. (9) to be relatively simple as a first step in applying our diagnostic framework in Section 1.

4.4. Maximum expected discharge

Eq. (9) describes the expected discharge from excess rainfall and does not include a base flow component. In river basins like GCEW, base flow is a minor component of streamflow during floods. Consequently, under these conditions the maximum of expected discharge from a single rainfall–runoff event can be expressed from (9) as

$$Q_{\mathrm{m}}(A) = \max_t E[Q_A(t)|D_1, \overline{D}_{2,A}] = \frac{E[Z|D_1]A}{\sqrt{2\pi(\sigma^2_1 + \bar{\sigma}^2_{2,A})}}, \tag{10}$$

where the subscript m means maximum and $\bar{\sigma}_{2,A} = cA^{\lambda}$. This equation shows that peak expected discharge depends on the shape of the excess-rainfall time series through σ_1 and on the shape of the response function through $\bar{\sigma}_{2,A}$. It does not depend on the times at which expected excess-rainfall and expected basin-response peak. Notice that $Q_{\mathrm{m}}(A)$ is the maximum of expected discharge and not the expectation of maximum discharge that Ogden and Dawdy [20] discussed and for which an analytical expression is more difficult to obtain.

Fig. 5 shows a log–log plot of $Q_{\mathrm{m}}(A)$ versus A using (10) where $E[Z|D_1] = 1.5$ cm, which is a typical excess-rainfall depth for a storm in GCEW, $\sigma_1 = 7$ and 43 min, and $\bar{\sigma}_{2,A} = 50.6\,A^{0.25}$ based on the observations presented in Fig. 4. The range of scales represented by the stream gauges in GCEW are highlighted along the x-axis in Fig. 5 and, across this scale range, each of the theoretical curves is approximately linear. This scale effect could explain the log–log linearity observed in data for the basin.

Table 1 provides a physical understanding of Eq. (10). It shows the asymptotic limits for $Q_{\mathrm{m}}(A)$ when $\sigma_1 \to \infty$ and when $\sigma_1 \to 0$. The first case represents a rainfall event of very long duration and relatively constant intensity. A steady-state relationship for $Q_{\mathrm{m}}(A)$ is obtained and occurs on the left side of the plotted curves in Fig. 5. The second case represents a rainfall event of very short duration. The limit for $Q_{\mathrm{m}}(A)$ depends on v because $\bar{\sigma}_{2,A} = cA^{\lambda}$ is inversely related to $1/v$; see Eq. (6). The limit is consistent with prior theoretical and numerical results which indicate that, for instantaneous excess rainfall, a power law relates peak-discharge to drainage area; e.g. [8,16]. In Fig. 5, this asymptotic condition appears on the right side of the plotted curves.

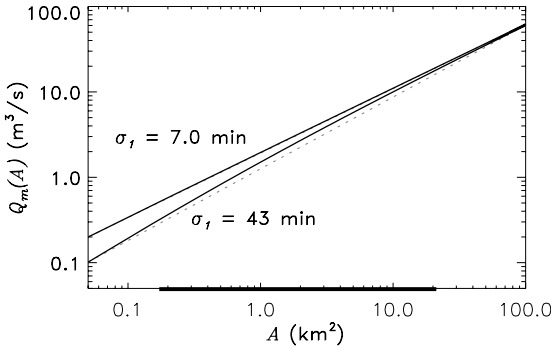

Fig. 5. Peak-discharge $Q_{\mathrm{m}}(A)$ versus A in log–log space based on Eq. (10) for $\sigma_1 = 7$ and 43 min, $E[Z|D_1] = 1.5$ cm, and $\bar{\sigma}_{2,A} = 50.6\,A^{0.25}$. A dotted straight line connects the endpoints of each theoretical curve to highlight its degree of curvature. The thick line on the x-axis depicts the range of spatial scales represented by stream gauges in GCEW.

Table 1
Asymptotic relations from Eqs. (10)–(12) where r_{p} equals the maximum over s of Eq. (3)

$\sigma_1 \to \infty$:	$Q_{\mathrm{m}}(A) \to r_{\mathrm{p}}n$
	$\theta \to 1$
	$\alpha \to r_{\mathrm{p}}/a$
$\sigma_1 \to 0$:	$Q_{\mathrm{m}}(A) \to (E[Z\|D_1]/\sqrt{2\pi}c)A^{1-\lambda}$
	$\theta \to 1-\lambda$
	$\alpha \to E[Z\|D_1]/\sqrt{2\pi}c$

Eq. (10) gives four general predictions about the mean relationships between $Q_m(A)$, A, and excess-rainfall in a basin. For streamflows sampled across a wide range of drainage areas within a basin, (1) a curve in log–log space will relate $Q_m(A)$ to A, and (2) the curve will approach a line of slope 1 as the duration of excess rainfall increases and the basin becomes saturated. If peak flows are sampled across a narrow range of spatial scales, as in GCEW, then (3) $Q_m(A)$ and A will be correlated as $Q_m(A) = \alpha A^\theta$ and (4) changes in α and θ among events will be caused by changes in mean excess-rainfall. Prediction (3) is supported by observed power law relationships [5,20].

5. Diagnosing observed peak-discharge power laws

As stated in Section 1, Furey and Gupta [5] observed the following trends among 148 events in GCEW:

1. For events with the same duration $\hat{\sigma}$, α increased and θ remained constant as depth $\hat{r}_d$ increased. The relationship between α and $\hat{r}_d$ was linear.
2. For events with the same depth $\hat{r}_d$, α decreased and θ increased as duration $\hat{\sigma}$ increased. These relationships were nonlinear.

We diagnose these observations below using our theoretical developments. In Section 5.1, we first formulate expressions for α and θ from Eq. (10) and discuss their physical meanings. In Section 5.2, we then examine the relationships between α, θ, and excess-rainfall, in the context of these expressions.

5.1. Power law parameters for maximum expected discharge between basins of different drainage areas

To derive expressions for the power law parameters α and θ, suppose that in log–log space a line connects peak-discharge at one scale, A, to peak-discharge at a larger scale, bA, where $b > 1$ is a constant. Then, the slope of this line is obtained from (10) as

$$\theta = \frac{\log Q_m(bA) - \log Q_m(A)}{\log bA - \log A} = 1 - \frac{\log\left(\sqrt{\frac{\sigma_1^2+\bar{\sigma}_{2,A}^2}{\sigma_1^2+\bar{\sigma}_{2,bA}^2}}\right)}{\log\left(\frac{1}{b}\right)}. \quad (11)$$

This equation is an approximation for θ obtained from data. It shows that θ is a function of spatial scale because (10) is not a power law. It depends on the time series of excess-rainfall through σ_1, on the response function at scale A through $\bar{\sigma}_{2,A} = cA^\lambda$, and on the response function at scale bA through $\bar{\sigma}_{2,bA} = c(bA)^\lambda$. Thus, values of θ can change between rainfall events because of changes in σ_1 and/or $\bar{\sigma}_{2,A}$ and $\bar{\sigma}_{2,bA}$. The later two terms can change between events because of a change in v, as seen by solving for $\bar{\sigma}_{2,A}$ in Eq. (6) in Section 4.2. Additionally, the intercept of the line in log–log space is $\log\alpha = \log Q_m(A) - \theta\log A$ and gives

$$\alpha = \frac{Q_m(A)}{A^\theta} = \frac{E[Z|D_1]A^{1-\theta}}{\sqrt{2\pi(\sigma_1^2+\bar{\sigma}_{2,A}^2)}}. \quad (12)$$

This equation shows that α can change between rainfall events because of changes in $E[Z|D_1]$, σ_1, or v through $\bar{\sigma}_{2,A}$. Table 1 shows the asymptotic limits for θ and α when $\sigma_1 \to \infty$ and $\sigma_1 \to 0$. These limits correspond to large and small excess-rainfall durations, respectively.

5.2. Diagnostics

To diagnose the trends observed by Furey and Gupta [5], theoretical expressions for θ and α have been derived above. Next, terms captured in these expressions that correspond to $\hat{r}_d$ and $\hat{\sigma}$ need to be identified. The term corresponding to $\hat{r}_d$ is $E[Z|D_1]$. It is first presented in Eq. (3) and is also found in (12). The term corresponding to $\hat{\sigma}$ is $\sqrt{2\pi}\sigma_1$. This term follows from the definition of $\hat{\sigma}$ as the depth of estimated excess-rainfall divided by its peak; see Section 2.2. Evaluating this same ratio for excess-rainfall from (3) gives $\sqrt{2\pi}\sigma_1$. Thus, $E[Z|D_1]$ and $\sqrt{2\pi}\sigma_1$ from our theoretical developments represent $\hat{r}_d$ and $\hat{\sigma}$ in the discussion of results presented below.

5.2.1. Predictions for fixed values of $\sqrt{2\pi}\sigma_1$ and $E[Z|D_1]$

When $\sqrt{2\pi}\sigma_1$ is fixed, Eq. (11) shows that θ is independent of $E[Z|D_1]$ and therefore remains constant as $E[Z|D_1]$ changes. Under the same condition, Eq. (12) shows that α changes among events only when $E[Z|D_1]$ changes and that α and $E[Z|D_1]$ are linearly related. These predictions agree with trend 1 from [5].

When $E[Z|D_1]$ is fixed, Eqs. (11) and (12) show that θ and α change non-linearly among events with a change in $\sqrt{2\pi}\sigma_1$. Fig. 6 shows these relationships for $E[Z|D_1] = 1.0$, 1.5, and 2.0 cm where $\bar{\sigma}_{2,A} = 50.6\,A^{0.25}$. Notice that different values of $E[Z|D_1]$ give different curves for α, but the same curve for θ. These predictions agree with trend 2 from [5] and next are compared directly to observations.

5.2.2. Diagnosing observations in GCEW for a fixed value of $E[Z|D_1]$

Values of c and λ in the power law $\bar{\sigma}_{2,A} = cA^\lambda$ are needed to diagnose observations using our theoretical predictions. Accordingly, they were obtained from the simulation results where link velocity was fixed to $v_l = 1$ m/s and hillslope velocity v_h varied among simulations; see Fig. 4. The relative influence of v_h on predicted values of θ and α was observed to determine if predictions improve as v_h values reflect flow conditions more realistically. Among the three values of v_h used in our simulations, $v_h = 0.1$ is the most realistic velocity for surface runoff on a hillslope; D'Odorico and Rigon [3] indicate that this value is an upper bound for hillslope velocity. Results from this investigation are discussed below along with the effects of varying link velocity.

Fig. 7 shows the observed relationships between θ and $\hat{\sigma}$ and predicted mean relationships based on (11). As v_h

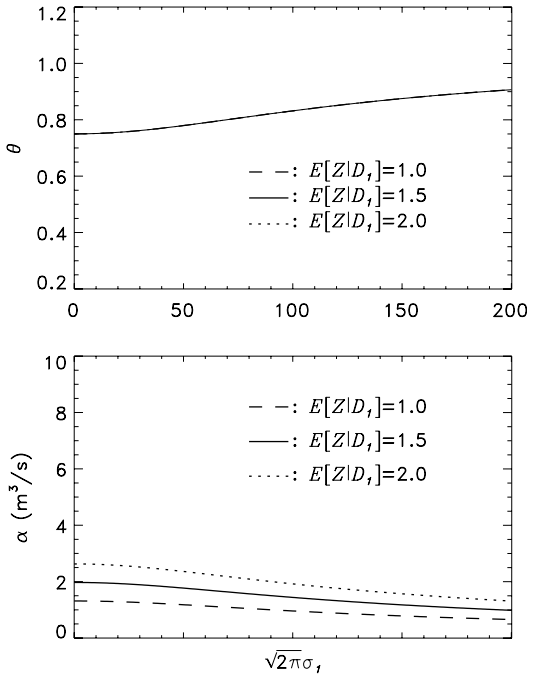

Fig. 6. The top plot shows θ versus $\sqrt{2\pi}\sigma_1$ according to (11). It shows that θ remains the same for different values of $E[Z|D_1]$; observations in [5] for realizations of $Z|D_1$ support this relationship. The bottom plot shows α versus $\sqrt{2\pi}\sigma_1$ according to (12). Here, α represents the peak-discharge that occurs at a drainage area of 1 km^2. Both plots were generated using the simulation result $\bar{\sigma}_{2,A} = 50.6\,A^{0.25}$ ($v_h = 0.1$, $v_l = 1.0$ m/s; see Section 3.3).

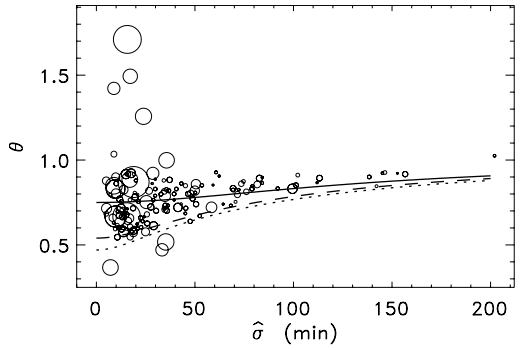

Fig. 7. Exponent θ versus $\hat{\sigma}$ for the 148 events examined in [5]. Each circle denotes an event and circle diameter represents the spatial CV of total rainfall for the event, as determined from the 31 rain gauges in GCEW. As circle diameter increases, so does the spatial variability in total rainfall; see [5]. The three curves are predicted by Eq. (11). For each curve, $b = 21.2/0.172 = 123$ is the ratio of the largest and smallest drainage areas among stream gauges in GCEW. The solid curve is based on the simulation result $\bar{\sigma}_{2,A} = 50.6\,A^{0.25}$ ($v_h = 0.1$, $v_l = 1.0$ m/s), the dashed curve is based on $\bar{\sigma}_{2,A} = 27.05\,A^{0.46}$ ($v_h = 1.0$, $v_l = 1.0$ m/s), and the dotted curve is based on $\bar{\sigma}_{2,A} = 23.51\,A^{0.53}$ ($v_h = \infty$, $v_l = 1.0$ m/s).

increases and parameters c and λ change, the predicted relationship between θ and $\hat{\sigma}$ is less consistent with observations. In the case where $v_h = \infty$ and there are no hillslope effects on streamflow response, the magnitude of θ is underpredicted for nearly all events. Thus, a better comparison between theory and observation is obtained when flow conditions are more realistic.

Fig. 7 indicates that errors in predicting a mean θ are greatest at low values of $\hat{\sigma}$. Under these conditions, θ depends largely on the value of λ because, as shown in Table 1, $\theta = 1 - \lambda$ when $\sigma_1 \to 0$. Therefore, at low values of $\hat{\sigma}$, it is critical to have a good estimate of λ to predict mean θ. This estimate must address both hillslope and network effects on routing water through a basin. If only network effects are addressed, which is the case where $v_h = \infty$, then λ will be too large to obtain a reasonable prediction. This is true for any physically realistic value of v_l. This result suggests that equating response duration to a network-based expression like Hack's Law, as done in [26], can lead to significant errors when investigating how peak streamflows scale with A in basins like GCEW. It also complements the finding in D'Odorico and Rigon [3] that hillslope velocity strongly influences the distribution of residence times of water in basins with relatively small drainage areas.

Fig. 8 shows observed relationships between α and $\hat{\sigma}$ and predicted mean relationships based on (12) where $\bar{\sigma}_{2,A} = 50.6\,A^{0.25}$. Each plot in the figure represents a narrow range of $\hat{r}_d$ values. Predictions are consistent with observations both with respect to trends and magnitudes. Interestingly, the predictions indicate that the variability in α at a given value of $\hat{\sigma}$ is caused largely by variability in $\hat{r}_d$. This variability decreases as $\hat{\sigma}$ increases. Also, notice that the middle plot consists of enough points to suggest the presence of a concave relationship between α and $\hat{\sigma}$. This relationship is speculative because of variability among the plotted points. But, it is predicted theoretically, though to a lesser degree than data shows in the middle plot.

Results suggest that trends in α and θ can be impacted by the dependence of v_h and v_l on excess-rainfall rate. For simplification, we have assumed that $v_l = 1.0$ m/s for all events, regardless of excess-rainfall conditions. However, a more realistic relationship is that, on average, v_l increases as excess-rainfall rate increases. This relationship means that v_l increases as both $\hat{r}_d$ is held constant and $\hat{\sigma}$ decreases because $\hat{r}_d/\hat{\sigma}$ represents the mean excess-rainfall rate for an event. Its effect on α was examined with respect to the middle plot in Fig. 8. Although not shown here, increasing v_l to 1.5 m/s raises the lefthand side of the theoretical curve in the plot and noticeably reduces the difference between the theoretical and empirical concave relationships. This increase in v_l has little impact on the theoretical relationship between θ and $\hat{\sigma}$ for small values of $\hat{\sigma}$. Similarly, v_h probably increases when excess-rainfall rate increases. Although not shown here, increasing v_h from 0.05 to 0.1 changes the lefthand side of the curve in the middle plot in Fig. 8 in the same manner as increasing v_l. Therefore, the relationship that v_h and v_l increase when excess-rainfall rate increases does impact theoretical trends in α and θ and could play an important role in the origins of observed power laws in GCEW.

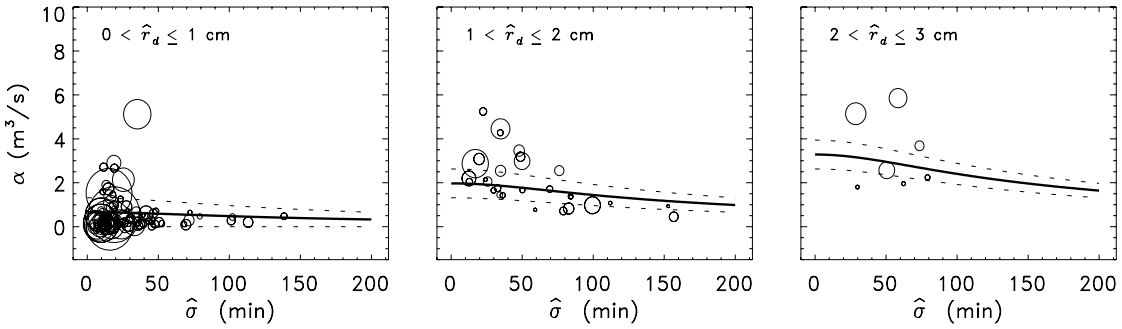

Fig. 8. Coefficient α versus $\hat{\sigma}$ for most of the 148 events examined in [5]; plots are conditioned on a narrow range of $\hat{r}_d$ values and events where $\hat{r}_d > 3$ cm are not shown. As in Fig. 7, circle diameter represents the spatial CV of total rainfall for an event. The curves are predicted by Eq. (12) using the simulation result $\bar{\sigma}_{2,A} = 50.6\,A^{0.25}$ ($v_h = 0.1$, $v_l = 1.0$ m/s). In each plot, the solid curve is for the middle value of $\hat{r}_d$ (e.g. $E[Z|D_1] = \hat{r}_d = 1.5$ in center plot). The dotted curves are for the bounds of $\hat{r}_d$ (e.g. 1 and 2 for lower and upper curves in center plot).

5.3. Theoretical limitations and extensions

A significant portion of the variability observed in the event-to-event values of α and θ is not accounted for theoretically. In particular, as shown in Fig. 7, θ varies greatly for small values of $\hat{\sigma}$. Observations in Furey and Gupta [5] indicate that this variability is likely caused by spatial variability in excess-rainfall, due to spatial variability in rainfall and/or soil-moisture. Spatial variability in excess-rainfall is not considered in our theoretical developments.

Our theoretical developments are also based on assuming that the expected time series of both excess rainfall and basin response are Gaussian density functions. This assumption provides a reasonable first-order representation for each type of time series in GCEW, as shown in Section 3. Under the same framework, other functions besides a Gaussian density could be used to define the expected excess-rainfall and basin-response function. For instance, a Gamma density could be used. In this case, the streamflow hydrograph could be skewed to the right, as data often suggest. If a Gamma density is used to develop a peak flow equation, the result, which is not shown here, is similar to Eq. (10).

Peak-discharge data can be used to estimate the expectation of peak-discharge but not the peak of expected discharge, which is the quantity expressed by (10). This distinction is underscored by the inequality $E[\max_i X_i] \neq \max_i E[X_i]$ where X_i, $i = 1, 2, 3, \ldots$, represents an arbitrary sequence of random variables. Therefore, a direct comparison between theory and data requires an equation for expected maximum discharge, but obtaining such an equation is difficult. Interestingly, as explained at the end of Section 4.2, our theoretical developments show that a power law relates the peak of the expected basin-response function to A. Similarly, Veitzer and Gupta [30] have shown empirically that a power law relates the expected value of the width function peaks to A. This similarity suggests that the steps needed to obtain an equation for expected maximum discharge could be comparable to those taken to develop (10).

The theoretical trends shown in Figs. 7 and 8 are based on a spatial sampling that is broader than the sampling represented by data. The relationship $\bar{\sigma}_{2,A} = cA^{\lambda}$ is obtained from simulation results for each of the 552 links that comprise the DEM-extracted river network of GCEW. Consequently, theoretical trends represent how mean peak-discharge changes throughout GCEW during a rainfall–runoff event. On the otherhand, observed values of α and θ represent peak-discharge trends among only 13 gauged locations in the basin.

Our developments are for event-based peak-discharges, but they might apply to peak-discharge quantiles. For example, Goodrich et al. [6] investigated the relationship between peak-discharge quantiles and drainage area using data that was separated into two distinct areal ranges, with a gap in between. A power law correlation between peak-discharge quantiles and area was observed for each range. Based on Fig. 5 discussed in Section 4.4, a shallow curve could connect the quantile data in the Goodrich et al. study, and a scale effect like the one illustrated in the figure could explain each of the observed power law correlations that were found.

Eqs. (10)–(12) describe how $Q_m(A)$, θ, and α when given D_1 are related to excess-rainfall depth $E[Z|D_1]$ and duration σ_1. Yet, for a given value of D_1, these equations do not characterize how $E[Z|D_1]$ and σ_1 are related to one another. For example, the two curves in Fig. 3 are generated using one value of $E[Z|D_1]$ and two different values of σ_1 which correspond to two different values of D_1. A more likely scenario is that $E[Z|D_1]$ changes when D_1 changes. Thus, our theoretical developments underscore the need to understand the relationship between $E[Z|D_1]$ and D_1 in a basin like GCEW. This depth-duration relationship is for excess-rainfall, in contrast to those for rainfall that are commonly found in engineering hydrology [14].

6. Conclusion

Based on mean features of estimated excess-rainfall time series and simulated basin-response functions in GCEW, a stochastic equation was formulated that relates expected discharge to the depth and duration of excess-rainfall and drainage area. An equation for maximum expected discharge was then obtained that is physically consistent with other peak-discharge expressions. This equation was used

to diagnose the observation that, on average, peak-discharge depends on drainage area as $Q(A) = \alpha A^{\theta}$ during single rainfall–runoff events in GCEW and that α and θ change from one event to the next.

Expressions for α and θ were derived from the peak-discharge equation and compared to observations. We found that these expressions are consistent with observations only when hillslope velocity v_h is given a physically realistic value. For instance, if $v_h \gg 0.1$ m/s, then the predicted trends relating α and θ to the depth and duration of excess-rainfall deviate from observed trends. This result suggests that equating response duration to a network-based expression like Hack's Law can lead to significant errors when investigating how peak streamflows change with A in basins like GCEW. It also complements the finding that hillslope velocity strongly influences the distribution of residence times of water in basins with relatively small drainage areas [3].

Observations and theoretical results indicate that if excess-rainfall depth $\hat{r}_d$ is fixed then there is a decreasing concave relationship between α and excess-rainfall duration $\hat{\sigma}$. Theoretical results predict a lower degree of concavity than suggested by data. The theoretical assumption that v_h and link velocity v_l are the same for all events could be the cause of this difference between theory and data. A more realistic relationship is that, on average, v_h and v_l increase as excess-rainfall rate increases. This relationship means that v_h and v_l increase as both $\hat{r}_d$ is held constant and $\hat{\sigma}$ decreases because $\hat{r}_d/\hat{\sigma}$ represents the mean excess-rainfall rate for an event. Preliminary tests indicate that the difference between the observed and theoretical relationships are reduced when v_h and v_l depend on excess-rainfall rate and that this dependance could play an important role in the origins of observed power laws in GCEW.

Our efforts to understand the physical origins of peak-discharge power laws observed in GCEW, including their temporal variability, are guided by a five-step diagnostic framework presented in Section 1. Step 5 is an assessment of how well the physical origin of the power laws are understood. If understanding is deemed inadequate then steps 2–5 can be repeated under different conditions. Based on the results in this paper, there are two limitations that standout in our understanding of the power laws in GCEW. First, we cannot adequately explain why the concave relationship between α and excess-rainfall duration becomes more pronounced as excess-rainfall depth increases. Two future objectives that address this issue are: (1) to examine the impact of more realistic hillslope and network routing conditions on α; and (2) to characterize the dependence between excess-rainfall depth and duration and then examine how this dependence influences α. Second, we have not explained the statistical variability around the trends shown in Figs. 7 and 8. Two future objectives that address this issue are: (1) to re-evaluate our estimates of excess-rainfall time series by using a more comprehensive model of surface infiltration; and (2) to assess excess-rainfall depth and duration for each event using unnested and spatially distributed estimates of these parameters.

Acknowledgement

Discussions with Ricardo Mantilla about using CUENCAS were very helpful in pursuing this research. Grants from the National Science Foundation supported this research and this support is gratefully acknowledged.

Appendix A

Notation introduced in Sections 1 and 2:

A	drainage area of a basin
$Q(A)$	peak-discharge observed in data or simulations
$q_p(A)$	annual streamflow quantile with return period p
$\hat{r}_d$	depth of estimated excess-rainfall for a rainfall–runoff event
$\hat{r}_p$	peak rate of estimated excess-rainfall for a rainfall–runoff event
α, θ	coefficient and exponent of the power law relating $Q(A)$ and A
$\hat{\sigma}$	measure of duration for estimated excess-rainfall; equals $\hat{r}_d/\hat{r}_p$

Notation introduced in Section 3:

L	longest-channel length in a basin
t	time
$q(t, A)$	simulated discharge at time t from a basin of drainage area A
$q_T(A)$	total volume of simulated discharge from a basin; equals 0.001 A
$\hat{r}(t)$	estimated excess-rainfall rate at time t for a rainfall–runoff event
v_h	velocity of runoff from a hillslope used in simulations
v_l	velocity of runoff from a link used in simulations
τ	measure of duration for simulated discharge; equals $q_T(A)/Q(A)$
c, λ	coefficient and exponent of the power law relating τ and A in simulations

Notation introduced in Sections 4 and 5:

a	mean area of hillslopes in a basin
b	constant (>1) defined as the ratio of two different drainage areas
D_1	random variable representing the duration of excess-rainfall for a rainfall–runoff event
$D_{2,A}$	random variable representing the duration of the basin-response function for a basin with drainage area A
$\overline{D}_{2,A}$	expectation of $D_{2,A}$
$f_1(t)$	normal density function with mean μ_1 and variance σ_1^2 that represents the expected shape of the time series of excess-rainfall when conditioned on D_1

$f_{2,A}(t)$ normal density function with mean $\mu_{2,A}$ and variance $\sigma^2_{2,A}$ that represents the expected shape of the response function for a basin of drainage area A when conditioned on $D_{2,A}$

$\bar{f}_{2,A}(t)$ normal density function with mean $\bar{\mu}_{2,A}$ and variance $\bar{\sigma}^2_{2,A}$ that represents the expected shape of the response function for a basin of drainage area A when conditioned on $\overline{D}_{2,A}$

l mean distance that a particle of water travels over a hillslope and through the adjoining network link in a basin

$Q_A(t)$ random variable representing streamflow discharge at time t from a basin of drainage area A

$Q_m(A)$ maximum over time t of the expectation of $Q_A(t)|D_1, \overline{D}_{2,A}$

n total number of links in a basin of drainage area A

$R(t)$ a stochastic process representing excess-rainfall rate at time t

T duration of a rainfall–runoff event

v effective velocity at which water travels over hillslopes and through network links in a basin

$W_A(t)$ a stochastic process representing the basin-response function at time t for a basin of drainage area A

Z random variable representing excess-rainfall depth for a rainfall–runoff event

References

[1] Alonso CV, Bingner RL. Goodwin Creek experimental watershed: a unique field laboratory, forum article. J Hydraul Eng 2000;March: 174–7.

[2] Blackmarr WA, editor. Documentation of hydrologic, geomorphic, and sediment transport measurements of the Goodwin Creek experimental watershed, Northern Mississippi, for the period 1982–1993, preliminary release, Res Report 3, Natl Sediment Lab, Agric Res Serv, US Dept Agric, Oxford, MS; 1995.

[3] D'Odorico P, Rigon R. Hillslope and channel contributions to the hydrologic response. Wat Resour Res 2003;39(5). doi:10.1029/2002WR001708.

[4] Eagleson PS. Dynamics of flood frequency. Wat Resour Res 1972;8(4):878–98.

[5] Furey PR, Gupta VK. Effects of excess-rainfall on the temporal variability of observed peak discharge power laws. Adv Wat Resour 2005;28:1240–53.

[6] Goodrich DC, Lane LJ, Shillito RM, Miller SN. Linearity of basin-response as a function of scale in a semiarid watershed. Wat Resour Res 1997;33(12):2951–65.

[7] Gupta VK, Castro SL, Over TM. On scaling exponents of spatial peak flows from rainfall and river network geometry. J Hydrol 1996; 187:81–104.

[8] Gupta VK, Waymire E. Spatial variability and scale invariance in hydrologic regionalization. In: Sposito G, editor. Scale dependence and scale invariance in hydrology. Cambridge: Cambridge University Press; 1998. p. 88–135.

[9] Gupta VK, Troutman BM, Dawdy DR. Towards a nonlinear geophysical theory of floods in river networks: An overview of 20 years of progress. In: Tsonis A, Elsner J, editors. Twenty years of nonlinear dynamics in geosciences. Springer Verlag, 2007 [In press].

[10] Hack JT. Studies of longitudinal profiles in Virginia and Maryland. US Geol Surv Prof Pap, 294-B; 1957.

[11] Klemes V. Guest editorial: of carts and horses in hydrologic modeling. J Hydrol Eng 1997;2(2):43–9.

[12] Lee MT, Delleur JW. A variable source area model of the rainfall–runoff process based on the watershed stream network. Wat Resour Res 1976;12(5):1029–36.

[13] Leopold LB, Wolman MG, Miller JP. Fluvial processes in geomorphology. New York: Dover Publications Inc.; 1992.

[14] Linsley RK, Kohler MA, Paulhus JLH. Hydrology for engineers. 3rd ed. New York: McGraw-Hill; 1982.

[15] Mantilla R, Gupta VK. A GIS numerical framework to study the process basis of scaling statistics in river networks. IEEE Geosci Remote Sens Let 2005;2(4):404–8. doi:10.1109/LGRS.2005.853571.

[16] Menabde M, Sivapalan M. Linking space-time variability of river runoff and rainfall fields: a dynamic approach. Adv Wat Resour 2001; 24:1001–14.

[17] Menabde M, Veitzer S, Gupta V, Sivapalan M. Tests of peak flow scaling in simulated self-similar river networks. Adv Wat Resour 2001;24:991–9.

[18] Mesa OJ, Gupta VK. On the main channel length-area relationship for channel networks. Wat Resour Res 1987;23(11):2119–22.

[19] Morrison JE, Smith JA. Scaling properties of flood peaks. Extremes 2001;4(1):5–22.

[20] Ogden FL, Dawdy DR. Peak discharge scaling in a small hortonian watershed. J of Hydrol Eng 2003;8(2):64–73.

[21] Parzen E. Modern probability theory and its applications. New York: John Wiley; 1960. 464 pp.

[22] Rodriguez-Iturbe I, Rinaldo A. Fractal river basins: chance and self-organization. New York: Cambridge University Press; 1997. 547 pp.

[23] Shreve RL. Variation of mainstream length with basin area in river networks. Wat Resour Res 1974;10(6):1167–77.

[24] Shreve RL. Infinite topologically random channel networks. J Geol 1967;75:178–86.

[25] Sivapalan M, Jothityangkoon C, Menabde M. Linearity and nonlinearity of basin response as a function of scale: discussion of alternative definitions. Wat Resour Res 2002;38(2). doi:10.1029/2001WR000482.

[26] Sólyom PB, Tucker GE. Effect of limited storm duration on landscape evolution, drainage basin geometry, and hydrograph shapes. J Geophys Res 2004;109:F03012. doi:10.1029/2003JF000032.

[27] Steiner M, Smith JA, Burges SJ, Alonso CV, Darden RW. Effect of bias adjustment and rain gauge data quality control on radar rainfall estimation. Wat Resour Res 1999;35(8):2487–503.

[28] Troutman BM, Karlinger MR. On the expected width function for topologically random channel networks. J Appl Prob 1984;21: 836–49.

[29] Troutman BM, Over TM. River flow mass exponents with fractal channel networks and rainfall. Adv Water Resour 2001;24:967–89.

[30] Veitzer SA, Gupta VK. Statistical self-similarity of width function maxima with implications to floods. Adv Wat Resour 2001;24: 955–65.